Proceedings of ASME Turbo Expo 2011
GT2011
June 6-10, 2011, Vancouver, Canada

GT2011-45588

Draft

A NUMERICAL INVESTIGATION OF ROTOR BOLT WINDAGE WITHIN A ROTOR STATOR CAVITY

Elham Roshani Moghaddam, Daniel Coren, Christopher Long and Abdulnaser Sayma

Thermo-Fluid Mechanics Research Centre
University of Sussex, Brighton, BN1 9QT, U.K.

ABSTRACT

This paper presents a numerical study of the effect of rotor mounted bolts on the windage within a rotor-stator cavity representative of modern gas turbine engine design. The CFD computations are performed using the commercial code FLUENT. The simulation methodology is first validated using experimental data from plain co-rotating disc and rotor-stator cavities from the open literature. Comparisons are then made with experimental data obtained from the bolt windage test rig at the Thermo Fluid Mechanics Research Centre (TFMRC), University of Sussex. Computations were performed at $Re_\phi = 6.8 \times 10^6$, $C_w = 5929$ ($\lambda_T = 0.35$) with different numbers of bolts ($0 < N < 60$), and also a continuous ring, at $r/b = 0.9$.

The study has improved the current understanding of the effect that rotor mounted protruding features have on windage in rotor-stator systems. It is seen that the contribution of skin friction to the moment coefficient reduces as the number of bolts is increased. The size and shape of the wake created by a rotating bolt also means that the pressure loss per bolt reduces with N but the overall effect is to increase the moment coefficient because there are more bolts.

NOMENCLATURE

a, b	Inner and outer radius of the disc, respectively
D	Bolt diameter (measured across-flats)
$G = s/b$	Gap ratio
M	Moment
$\dot{m}$	Mass flow rate
N	Number of bolts
p	Pressure
r_s	Radius of the shaft
r, z	Radial and axial coordinates
r_p	Radius of the protrusions
s	Axial gap between discs
s_c	Seal clearance
U	Mean radial velocity
V_r, V_ϕ	Radial and tangential velocities in a stationary coordinate system.
$\beta = V_\phi/\omega r$	Core rotation factor
β^*	Value of β when $C_w = 0$
μ	Dynamic viscosity
ρ	Density
ω	Angular velocity

Fluid Dimensionless Groups

$C_m = \dfrac{M}{1/2\,\rho\omega^2 b^5}$	Moment coefficient
$C_w = \dfrac{\dot{m}}{\mu b}$	Flow Reynolds number
$Re_\phi = \dfrac{\rho\,\omega\,b^2}{\mu}$	Rotational Reynolds number
$\lambda_T = \dfrac{C_w}{Re_\phi^{0.8}}$	Turbulent flow parameter

1 INTRODUCTION AND REVIEW OF PREVIOUS WORK

Increasing the efficiency of a gas turbine engine requires either a higher turbine entry temperature of the main gas flow or a reduction of internal losses. Turbine entry temperatures on modern civil engines are currently above 1600°C, and components in contact with such high temperatures quickly exceed their creep and fatigue limits. It is only possible to operate at these elevated temperatures because of internal air systems which use some of the compressor air to cool the turbine discs, blades and nozzle guide vanes. However, air used for cooling will be heated by viscous dissipation as it flows over both rotating and stationary surfaces. This parasitic phenomenon is referred to as *windage*. The magnitude of windage heating may also be expected to increase when features such as protrusions are fixed to the surface. More accurate windage predictions offer potential for improved design of the internal air system, with associated increases in thrust and efficiency.

Early investigations of windage losses due to rotating discs were carried out by Daily and Nece (1960) and Bayley and Owen (1969). These identified a number of relevant dimensionless parameters. For a disc of outer radius, b, rotating at an angular velocity ω, in a fluid of density ρ, and dynamic viscosity μ, supplied with a superimposed mass flow rate $\dot{m}$, the windage torque is M. The dimensionless flow rate, C_w, rotational Reynolds number, Re_ϕ and moment coefficient, C_m are defined as.

$$Re_\phi = \frac{\rho \omega b^2}{\mu} \tag{1}$$

$$C_w = \frac{\dot{m}}{\mu b} \tag{2}$$

$$C_m = \frac{M}{1/2\,\rho\omega^2 b^5} \tag{3}$$

For no superimposed flow, $C_w = 0$, the flow structure comprises separate boundary layers on the rotor and stator and a central core region where there is only tangential motion with about 40% of disc speed. Flow is pumped up the rotor and moves radially inward down the stator. For $C_w > 0$, increasing the superimposed flow reduces the tangential velocity of the core. For small amounts of superimposed flow, the flow structure in the cavity is dominated by rotation; conversely for large amounts, the flow structure is dominated by the superimposed flow. Owen and Rogers (1989) developed a useful parameter to delineate these two regimes. This is the turbulent flow parameter λ_T which takes its definition from Von Kármán's (1921) solution (using a one-seventh power law for the velocity profile) for the flow entrained by a free disc.

$$C_{w,ent} = 0.219\, Re_\phi^{0.8} \tag{4}$$

and so

$$\lambda_T = \frac{C_w}{Re_\phi^{0.8}} \tag{5}$$

For $\lambda_T > 0.219$, the flow structure is expected to be dominated by the superimposed flow and for $\lambda_T < 0.219$, rotational effects dominate.

Dibelius et al. (1984) investigated the effects of protrusions on windage. They used a test rig with a rotor disc in an enclosed housing, for rotor mounted bolts they noted a significant increase in the moment coefficient above that of a plain disc. This occurred for both zero superimposed flow and large values of superimposed flow. They also noticed that the effect of the protrusions on the flow structure was more pronounced when the flow was dominated by rotational effects.

Zimmerman et al. (1986) measured the effect on shaft torque of various bolt designs. Those considered were: staged (i.e. axially stacked concentric bolts of reducing diameter), cylindrical rotor bolts, partially covered and fully covered (by an annular ring) rotor bolts. It was found that eighteen staged bolts on a disc at a radius ratio, $r_p/b = 0.75$, increased torque by a factor of 2.5, with further increases for cylindrical shaped bolts. Partially covered bolts, gave little benefit in reducing windage compared to the uncovered bolts. However, fully covered bolts, gave a significant reduction in moment coefficient compared with the uncovered bolts and a moment coefficient of approximately 25% above that of a plain disc. The effect of a superimposed flow of $C_w = 2.6 \times 10^4$ was to increase the windage by 50% for all configurations. The increased windage due to protrusions was attributed to the superposition of three elements: form drag; boundary layer losses and pumping losses. They found that for a small number of bolts, form drag dominates the additional moment produced, whereas for a large number of bolts the pumping losses become more important. In addition, they also suggested a theoretical limit where increasing the number of bolts will decrease the amount of moment coefficient.

The experiments of Millward and Robinson (1989) involved varying the number of bolts, their diameter, circumferential pitch, and projected cross sectional area. These bolts were attached to both the rotor, as well as on the stationary casing. They obtained a correlation of their results for protrusions attached to the rotor. They also noted that the effect on windage of bolts located towards the outer radius was very significant, whereas those located towards the inner radius had little effect. For protrusions on the stator, there was insufficient data to derive a correlation, though a recommendation was made that stator bolts contributed one third of the windage of the corresponding rotor bolts. Tests were also carried out with full and partial covering of both stator and rotor bolts. No measurable effect was found by partially covering the rotor bolts but the stator bolts showed a reduction in windage at high mass flows. Fully covered bolts however, gave similar windage to a plain disc, and in some cases a reduction in windage was actually observed.

Gartner (1997) developed a semi-empirical correlation that gives satisfactory agreement for the moment coefficient from a plain disc over a wide range of dimensionless mass flows. Gartner (1998) used a momentum integral method to predict the windage torque from a single disc with protrusions. The predictions agree well with available data, providing the spacing between the bolts is not so small that wake effects become significant.

Coren (2007) carried out an experimental study on windage effects in rotor-stator cavities. Tests were carried out with bolts mounted on the rotor or on the stator. He suggested correlations for the windage heating as a function of the number, size and location of the bolts. He also used Laser Doppler Anemometry (LDA) to measure the radial and tangential components of velocity.

2 THE BOLT WINDAGE TEST RIG

Figure 1 shows a general assembly of the test rig. This consists of a shaft mounted titanium alloy disc of outer radius b = 225 mm enclosed within a sealed steel pressure casing. The maximum clearance between the rotor and casing, s = 22 mm. Around the outer rim of the disc is a labyrinth seal and a stator mounted shroud encases the cavities on either side of the disc. The disc is driven by a 50 kW motor through a 5:1 step up gearbox. Mounted between the gearbox and the disc is an in line torquemeter. The test side of the disc (labelled 'front cavity' in Figure 1) carries the majority of the instrumentation whereas the balance side (labelled 'rear cavity') has sufficient instrumentation to balance the flow conditions on both sides of the disc. A superimposed flow of air enters the rig centrally on the test side, flows radially outward through the cavity and leaves through the labyrinth seal at the perimeter. An equal amount of air is supplied to the balance side, where the air enters through four inlet pipes equally spaced around the central shaft. There are four orifice plates positioned upstream and downstream of the test rig on both the test and balance side to measure the mass flow of air through the rig as well as to ensure both sides are balanced. The air is supplied at pressures of up to 7.5 bar (absolute) and mass flows of up to 0.82 kg/s by an Atlas Copco screw type compressor and treated with an Atlas Copco air conditioning unit to provide dry air in the range 15 to 25 ºC prior to delivery to the rig.

A shaft mounted Vibrometer TM112 in line torquemeter measures torque and rotational speed. For the torque measurement, this has a sensitivity of 25 mV/Nm and the speed signal has a sensitivity of 0.2 mV/rev/min. The torque due to bearing friction in the test rig depends on rotational speed and was obtained by a previous calibration. This driveline torque was subtracted from all of the measured values of torque to obtain a value of the windage torque, M. The magnitude of the driveline torque varied from 2% of the total at high rotational speeds to 20% at low values of rotational speed.

Tests were carried out with N = 3, 9 and 18 and D = 16 mm, hexagonal bolts of height, H = 11 mm. These were attached, at a radius of 0.2 m, r_b/b = 0.889, to both sides of the disc surface to ensure similar conditions on either side, minimizing axial conduction. The orientation of the bolts relative to the direction of rotation is shown in Figure 2.

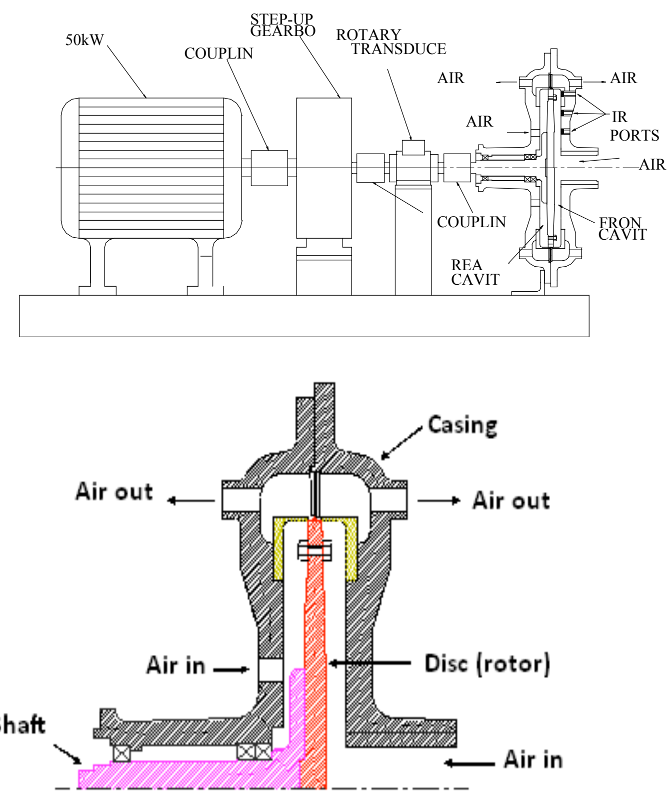

Figure 1. Schematic Diagram of the Bolt Windage Test Rig

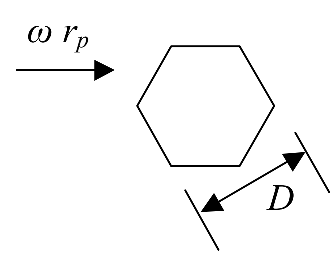

Figure 2 Orientation of Bolts with Respect to Rotation.

3 VALIDATION OF THE COMPUTATIONAL MODEL

Two cases were selected for validation purposes in this study. This choice was based on various considerations, such as similarity in geometric configuration and flow conditions with the actual bolt windage test cases as well as the availability of experimental data.

3.1 Validation Case No. 1: Flow in a rotating cylindrical cavity with radial outflow

The experimental data for this validation test case come from Pincombe (1981). Figure 3 shows a schematic diagram of the rotating cylindrical cavity comprising two co-rotating discs of outer radius b = 443 mm and separated by an axial distance s = 59 mm (G = s/b = 0.133). Air at 1 bar and 293 K enters the cavity axially with no swirl through a circular hole of radius a = 44.3 mm (a/b = 0.1) and leaves the cavity radially through an opening in the shroud. The dimensionless conditions investigated were: $Re_\phi = 10^5$ and $C_w = 1092$. In the experiment, there is peripheral shroud which has 30 holes of 32 mm diameter. For simplicity of modeling, the exit geometry is assumed to be a continuous slot of the same equivalent area as the thirty discrete holes. Figure 4. shows the 3-D configuration of the simulated geometry.

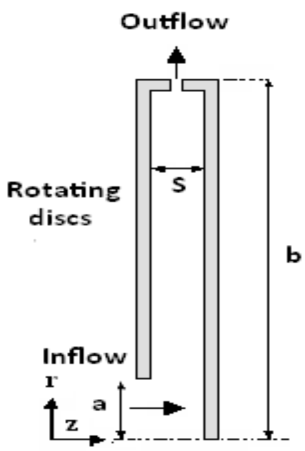

Figure 3 Schematic Diagram of Validation Test Case No. 1: Rotating Cylindrical Cavity with Radial Outflow

The simulation work for the bolt windage rig is non-axisymmetric. Consequently, all the validation test cases were simulated in 3-D. For the cavity shown here a 10° sector was modeled. As shown in Figure 4, there is an extended geometry after the outlet which is used to avoid reverse flow. This extended geometry provides a uniform flow before the outlet boundary, and prevents it from changing direction and re-entry through the outlet, which could cause numerical problems.

It is common to use an inlet pipe at the entrance of rotating cavities with superimposed flow. The role of this inlet pipe is to provide a fully-developed, low-turbulence velocity profile before entering the cavity. The length of the inlet pipe used here is 1.8 m.

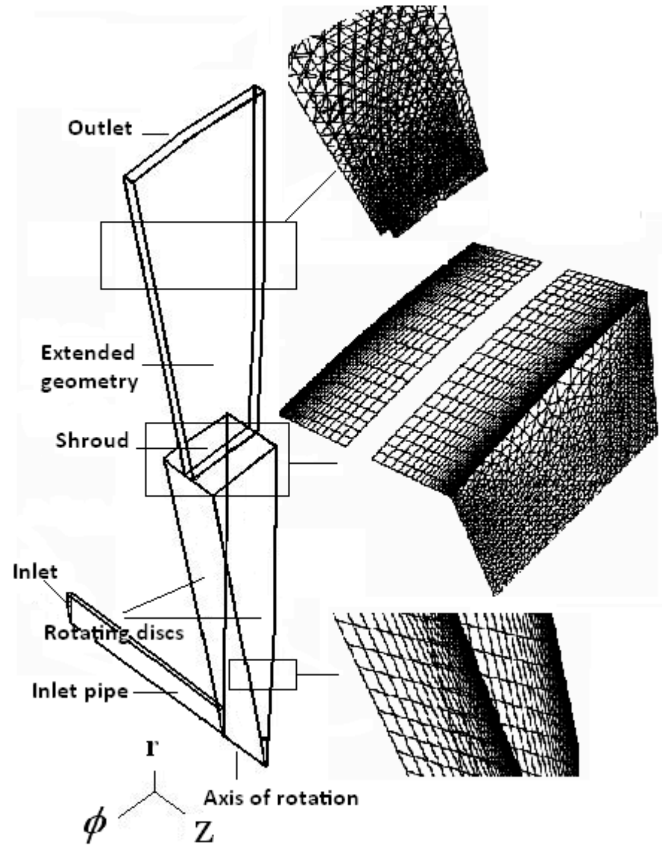

Figure 4 The Numerical Grid for Validation Test Case No. 1

A grid independence study was carried out in order to make sure that the computational results do not change by producing further refined grids (the finest mesh had 270,000 points)

As shown in Figure 4, unstructured meshes were only used in the plane of the disc surfaces (the r - ϕ plane). Meshes were generated for use with a low Reynolds number turbulence model in which the first grid near the wall is located in the laminar sub-layer region. The inlet velocity, outlet pressure and rotational speed were calculated from the values of mass flow coefficient and rotational Reynolds number. At the rotational speed of the test rig (7.6 rad/s) the flow can be assumed to be incompressible. Three thousand iterations were required to get a converged solution.

As described by Pincombe, for $C_w = 1092$, the flow is expected to be completely turbulent. Therefore the computational results are dependent on the selection of an appropriate turbulence model of the Reynolds Averaged Navier-Stokes equations are used. Accordingly, different turbulence models were examined in order to find the model which can best match the experimental data.

Figure 5 shows the axial variation (z/s = 0 corresponds to the surface of the upstream disc) of the radial component of velocity for a number of different turbulence models together with the experimental results of Pincombe. The radial velocity is shown in dimensionless form on the vertical axis as Vr/U where U is a mass-continuity derived radial velocity, defined by:

$$U = \frac{C_W \mu}{2\pi \rho r G} \qquad (6)$$

and the horizontal axis is the dimensionless axial coordinate z/s

As shown in Figure 5, all the turbulence models predict a similar radial velocity distribution across the cavity with differences that are thought to be within the bounds of experimental uncertainty. However, there is a noticeable difference between the predicted and measured values; the experimental results that show a higher maximum radial velocity and a steeper gradient towards the core region. The reason for this is unclear. However the following facts should be noted: the absolute values of this disparity are very small (less than 0.08 m/s); the measurement of this component of velocity is sensitive to small misalignment; the disparity with a $1/7^{th}$ power law is much greater; and the measurements were made almost thirty years ago with equipment that has been superseded.

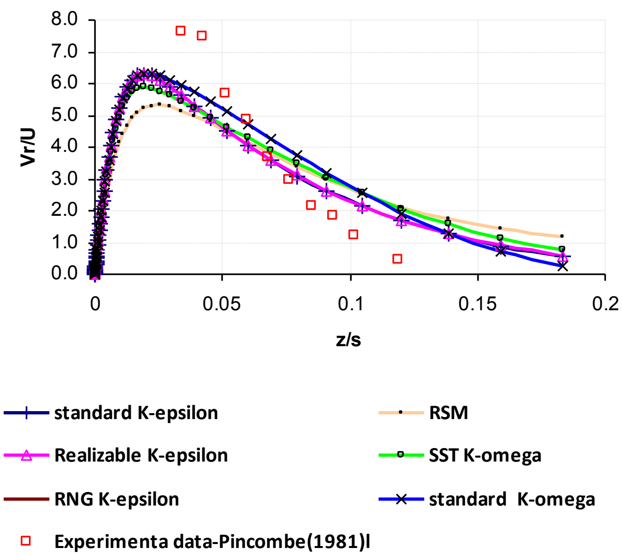

Figure 5. Validation Test Case No. 1. Axial Variation of radial velocity at r/b=0.833 using Different Turbulence Models and Comparison with Experimental Data.

Model	$V_\phi / \omega r$
Experimental data	0.29
Standard $k-\varepsilon$	0.35
Realizable $k-\varepsilon$	0.35
RNG $k-\varepsilon$	0.35
Standard $k-\omega$	0.35
SST $k-\omega$	0.35

Table 2: Validation Test Case No. 1 Comparison between the Tangential Velocity at r/b=0.833 and z/s = 0.5 for Different Turbulence Models

Table 2. shows the predicted values of dimensionless tangential velocity $V_\phi/\omega r$ at z/s = 0.5 (in the central core) and at r/b = 0.833 for different the turbulence models used. As can be seen the predictions of all turbulence models are similar, but the predicted values always exceed that measured experimentally. However, as previously noted the difference in velocity is small (0.17 m/s) in this case and the experimental uncertainties could be relatively significant.

3.2 Validation Test Case No. 2: Flow in a Rotor-Stator Cavity with a Superimposed Radial Outflow

This validation test case examines the flow in a fully shrouded rotor-stator system with a superimposed radial outflow of fluid. Comparison is made with the experimental measurements and computations of Poncet et al. (2005), who used water as the working fluid. The temperature was maintained constant at 23°C, the density and kinematic viscosity of water are taken as 999 kg/m³ and 0.942 10^{-6} m²/s respectively. Their measurements were obtained using a two-component Laser Doppler Anemometry system. Measurements were made of the radial and tangential components of velocity for both a superimposed radial inflow and a superimposed radial outflow. However, only the results of the case with radial outflow are used for comparison in this present study. Figure 6 shows a schematic diagram of the cavity where: s = 9 mm, b = 250 mm (G = s/b = 0.036), a = 54.5 mm, r_s = 38 mm and s_c = 3 mm. The comparison here is for $Re_\phi = 1.04 \times 10^6$ and C_w = 5929 (λ_T = 0.09).

In the experiment, water enters axially through the stator and leaves the cavity axially through a radial gap between the rotor and the shroud. The disc adjacent to the inlet (stator) and the shroud are stationary, while the rotor and the shaft are rotating.

In addition to the experimental measurements, Poncet et al. used a numerical method for computing the radial and tangential components of velocity. They used a RSM model which is based on one-point statistical modeling using a low Reynolds number second-order full stress transport closure.

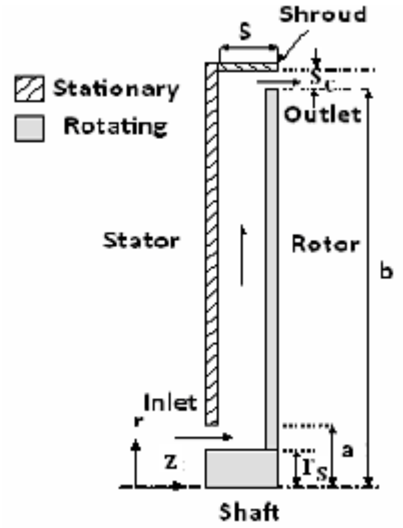

Figure 6. Validation Test Case No. 2, Schematic Configuration of the Cavity with Relevant Notation

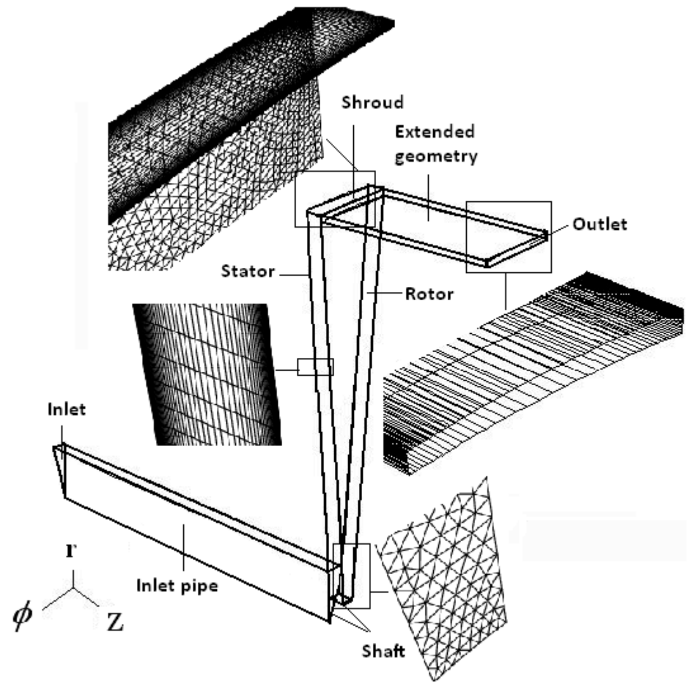

Figure 7. The Numerical Grid for Validation Test Case No. 2

Figure 7. shows the 3D geometry of the mesh used to simulate the flow in this rotor stator cavity. As in the previous test case, a 10° sector is simulated. The simulated cavity also has extended geometry at the outlet (for eliminating reverse flow at the exit boundary) and an attached pipe at the inlet (to provide the fully developed flow conditions).

Figure 8 and 9 compare the current computational results for the axial variation of dimensionless radial and tangential velocities, respectively, at r/b = 0.56 with the experimental and numerical results of Poncet et al. The horizontal and vertical axes of Figure 8 are as defined before (z/s and v_r/U, respectively); z/s = 0 corresponds to the surface of the stator, and z/s = 1 the rotor. For Figure 9, the vertical axis is the nondimensional tangential velocity or swirl ratio, V_ϕ / ωr.

The standard K-ε, the realizable K-ε, and the RSM give the closest results to the experimental data. The standard K-ε model was chosen for all further computations due to the lower overhead in processing time. The radial and tangential velocities at two other radial locations of r/b = 0.44, and r/b = 0.8 are shown in Figure 8 to 13 for the standard K-ε, turbulence model.

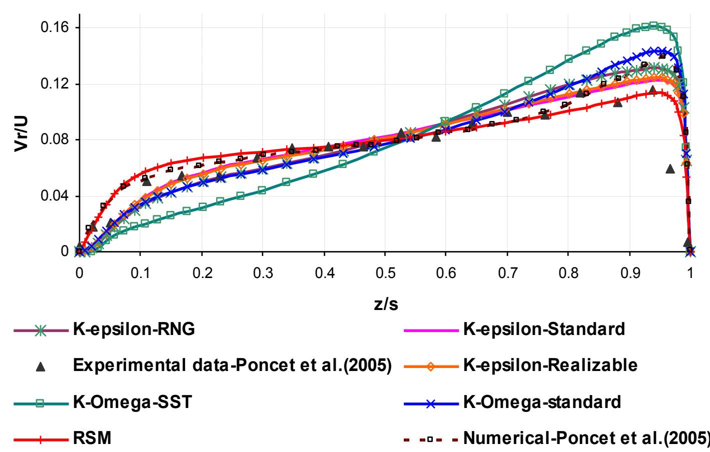

Figure 8. Axial Variation of Radial Velocity at r/b = 0.56 Using Different Turbulence Models.

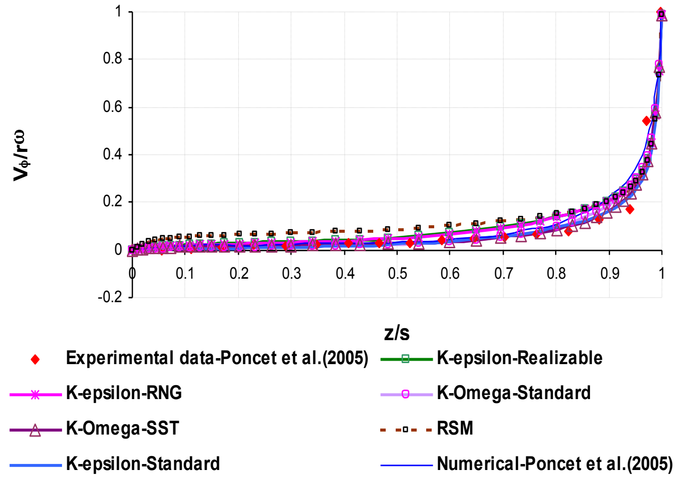

Figure 9. Axial Variation of Tangential Velocity at r/b = 0.56 Using Different Turbulence Models.

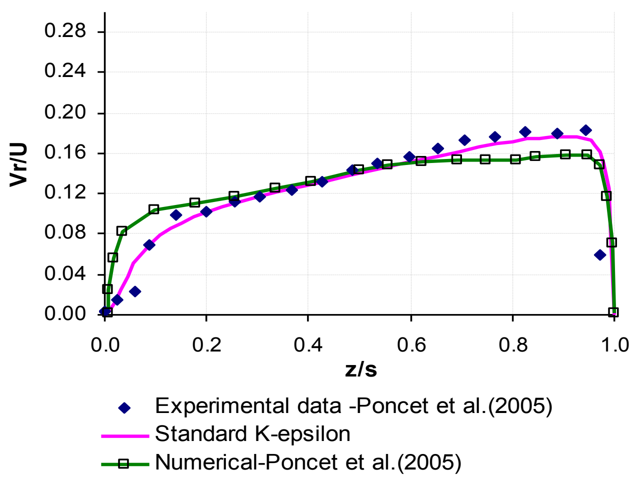

Figure 10. Axial Variation of Radial Velocity at r/b = 0.44.

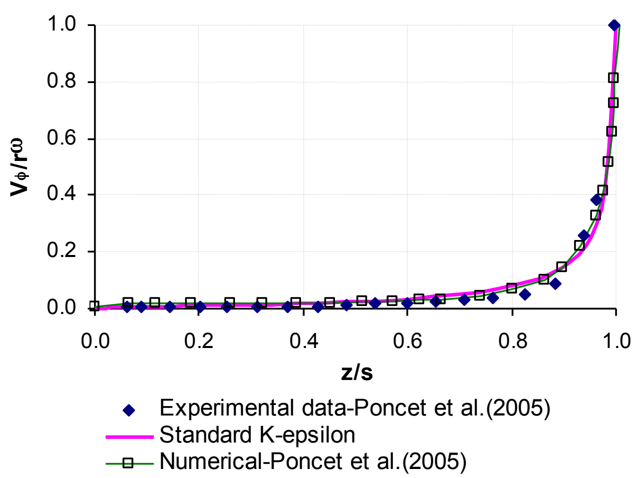

Figure 11. Axial Variation of Tangential Velocity at r/b = 0.44

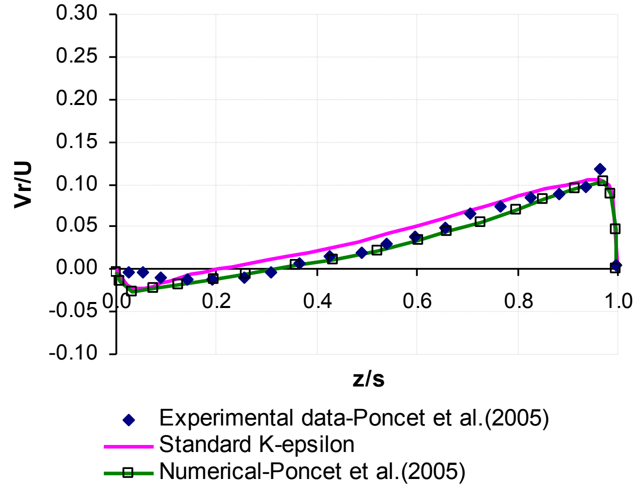

Figure 12. Axial Variation of Radial Velocity at r/b = 0.8.

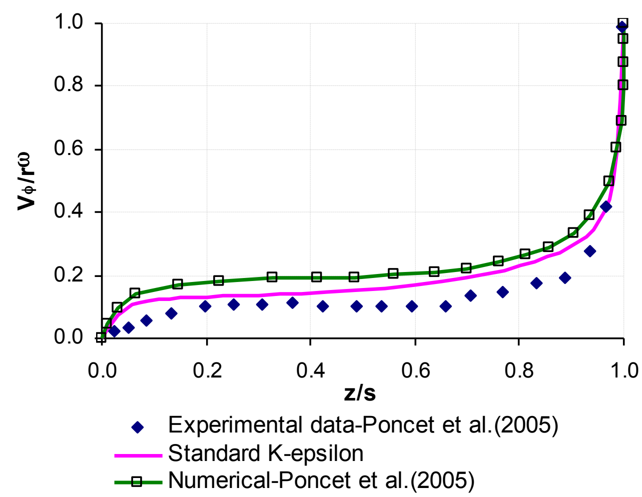

Figure 13. Axial Variation of Tangential Velocity at r/b = 0.8.

The current numerical predictions are in acceptable agreement with both the experimental data on Poncet et al. and also their numerical predictions. Looking at the results shown in Figures 8 to 13 also illustrates some important features of this rotor-stator flow regime. For r/b = 0.56 and 0.44 (Figures 9 and 11) there is not a tangential velocity boundary layer on the stator and only on the rotor. The radial velocity at these locations shows evidence of radial outflow only and no recirculation radially inward back down the stator. These features are consistent with what is called a Stewartson Type flow regime. At r/b = 0.8 (Figures 12 and 13), this Stewartson Type flow becomes a Batchelor Type flow where there are separate boundary layers on the rotor and stator. Fluid moves radially outward in the rotor boundary layer and radially inward in the stator boundary layer. In Figure 13, there is clear evidence of a core region between the rotor and stator ($0.2 < z/s < 0.8$). The tangential velocity in the core region is usually denoted by the symbol β. For the current numerical predictions at $r/b = 0.8$, $\beta = 0.16$ (the experimental results of Poncet et al. give $\beta = 0.2$ and their numerical predictions give $\beta = 0.11$).

4. THE NUMERICAL MODEL OF THE BOLT WINDAGE RIG

Figure 14 shows part of the 3-D mesh used in the computational model for the bolt windage test rig. The angular extent of the sector simulated depends on the number of bolts. The periodic boundaries of this sector lie mid-way between the bolts, so for 3 bolts a 120° sector is used, for 9 bolts a 40° sector and for 18 bolts a 20° sector. There is an extended geometry at the outlet, and a pipe attached to the inlet. Unstructured grids were used in the r-ϕ plane only. Finer grids are used near the bolt. The distance near the walls were specified so that using the low Reynolds number approach is possible. The k-epsilon (standard) model was used for simulations. The pressure and temperature at inlet were set from the experimental data. The outlet pressure was set so that it produces the amount of fixed mass flow rate. A moving reference frame with an angular velocity of the rotor speed was used.

The results shown in this paper are for air with a mass flow of 0.415 kg/s, a rotational speed of 409.5 rad/s an inlet pressure of 5 bar and temperature of 296.7 K The equivalent dimensionless conditions are: $Re_{\phi} = 6.8 \times 10^6$, $C_w = 10^5$, corresponding to $\lambda_T = 0.35$.

5 ANALYSIS OF RESULTS

Figure 15 shows the variation of moment coefficient (on one side of the disc) with number of bolts N. The experimental results, together with those from the CFD simulations are shown for N = 3, 9 and 18 bolts as well as for a plain disc. The plain disc results are indicated by a continuous line for the experimental data and a dashed line for the CFD predictions. Both experimental data and CFD predictions show that, not surprisingly, increasing the number of bolts causes a significant rise in the moment coefficient. As can also be seen from the results shown in Figure 15, there is good overall agreement between the predictions and experimental data and this gives confidence in the numerical model.

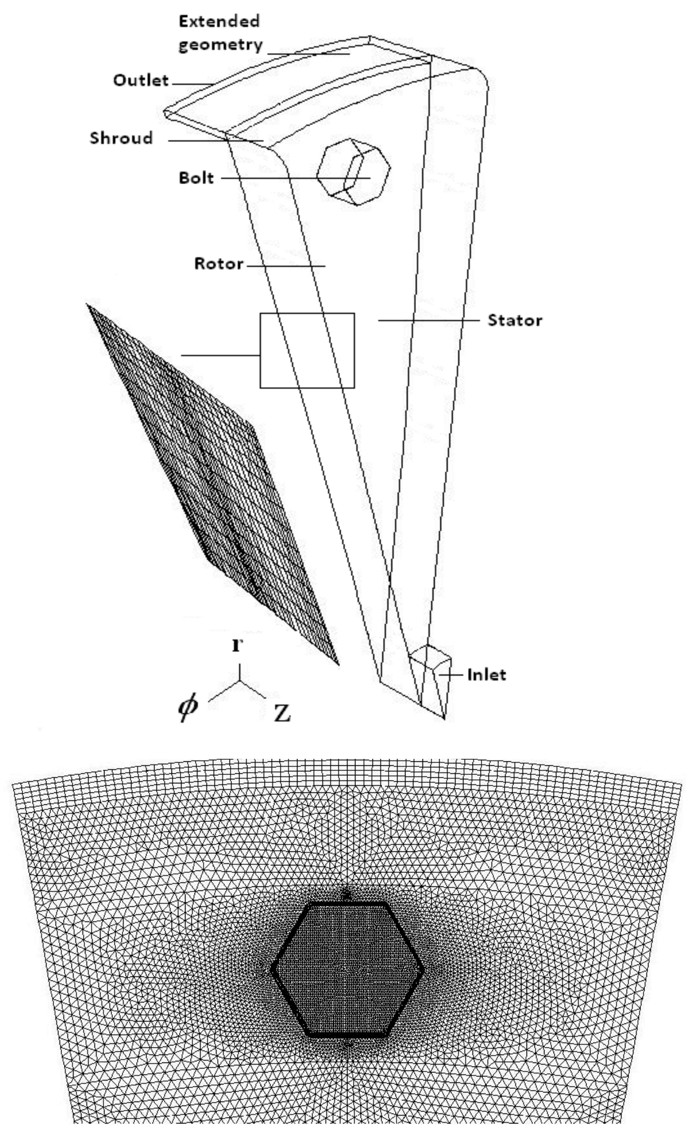

Figure 14. A Section of the Computational Mesh used for the Bolt Windage Test Rig

Further simulations were carried out for N = 36, 45, 52 and 60 (for N = 60, the circumferential spacing between one bolt and the next is less than D/4) and a continuous ring with 16 mm radial thickness and 11 mm height at r = 0.2 m on the rotor. These results are summarised in Figure 16, which again shows the variation of moment coefficient with N.

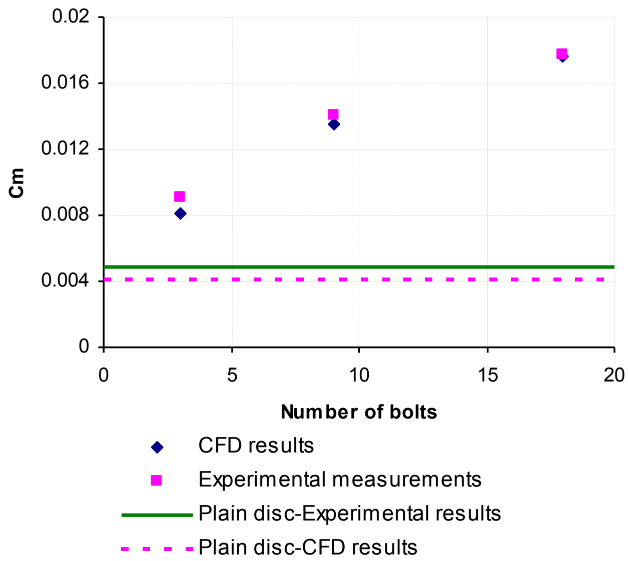

Figure 15. Variation of Moment Coefficient with Number of Bolts N. Comparison Between Numerical and Experimental Results for 3, 9 and 18 bolts and also a plain disc: Re, = 6.8 x 10^6, $C_w = 10^5$ ($\lambda_T = 0.35$).

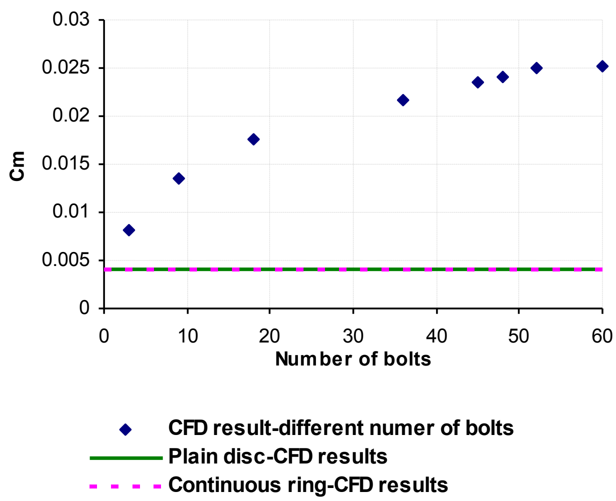

Figure 16. Predicted Variation of Moment Coefficient with Number of Bolts, N for Re, = 6.8 x 10^6, $C_w = 10^5$ ($\lambda_T = 0.35$).

The CFD results shown in Figure 16 extend the range of those shown in the previous figure and provide a consistent picture of the effect of the number of bolts on the moment coefficient. It is interesting to see from Figure 16 that the moment coefficient of the ring (at N = 0) is approximately equal to the moment coefficient of a plane disc. This is in agreement with the investigations of Millward and Robinson (1989).

The effect of the number of bolts on the axial variation of dimensionless tangential velocity is illustrated in Figure 17. The tangential velocity varies around the circumference of the bolt radius. The value used in this graph is that obtained at the location of the centreline of the bolt.

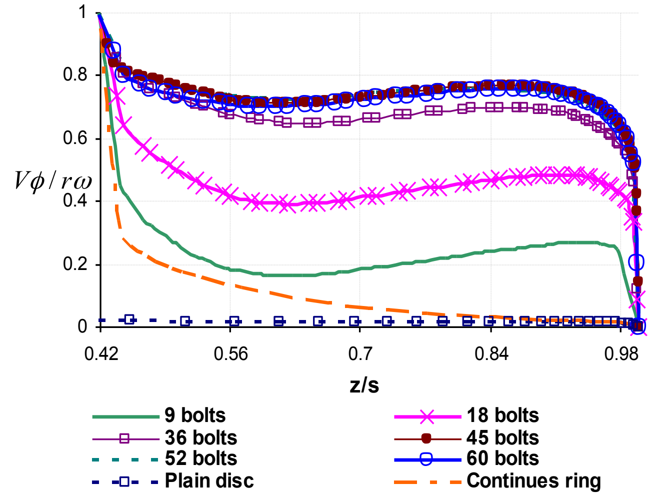

Figure 17. Predicted Axial Variation of Dimensionless Tangential Velocity at r/b = 0.9, Re, = 6.8 x 10^6 and $C_w = 10^5$ ($\lambda_T = 0.35$).

It can be seen from Figure 17 that increasing the number of bolts from 9 to 36 causes a significant increase in the tangential velocity. The corresponding change from 36 to 60 bolts is much less and there is very little difference in the tangential velocity when $N \geq 45$. Increasing N is expected to reduce the contribution of skin friction to the total losses since the relative velocity between the fluid and the bolt is reduced.

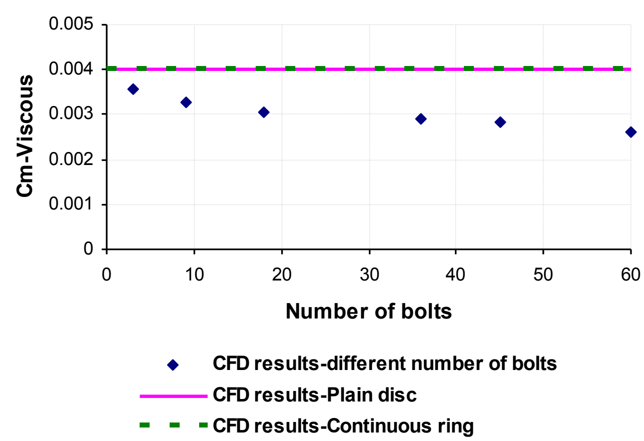

Figure 18 Variation of Moment Coefficient due to Skin Friction with Number of Bolts, Re, = 6.8 x 10^6 and $C_w = 10^5$ ($\lambda_T = 0.35$).

This later point can be examined by considering just the contribution of skin friction to the total loss. And this is shown in Figure 18, which shows the variation of skin friction based moment coefficient with number of bolts. The results agree with the statement made above; the moment produced by skin friction decreases with increased number of bolts.

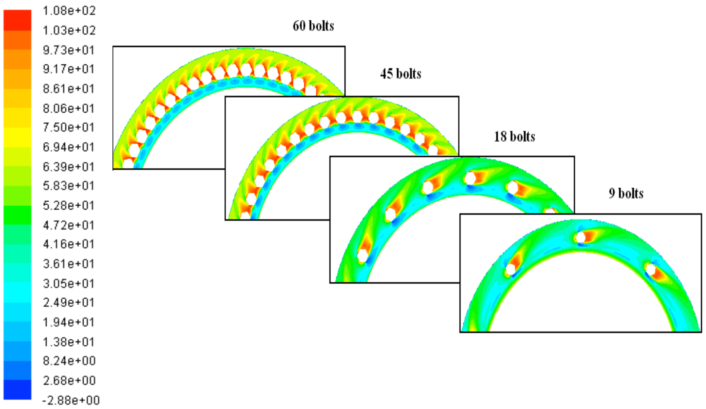

Figure 19. Tangential velocity Contours around the Bolts for N = 9, 18, 45 and 60 (Re, = 6.8 x 10^6 and C_w = 10^5).

Similar trends occur when the turbulent flow in the wake behind the bolts is examined. This can be seen from Figure 19 which shows contours of tangential velocity in the region of the bolt radius. It is apparent that the form of the wake changes with the number of bolts fitted to the rotor. Increasing the number of bolts (and decreasing the distance between the two neighbouring bolts) can lead to a situation where the wake of one bolt has not fully collapsed in advance of the following bolt. Although only one condition has been investigated here (Re, = 6.8 x 10^6 and C_w = 10^5, λ_T = 0.35), it is likely that the interference of the wake from one bolt to the next will be dependent on λ_T. This subject will be investigated and reported on in a future publication.

Figure 20 shows contours of total pressure in the region of the bolt radius for N = 9, 18, 45, and 60. It is clear that increasing the number of bolts, increases the peak total pressure but also decreases the pressure difference across each individual bolt. This leads to a net decrease in the moment due to a single bolt as a consequence of the increased influence of wakes from upstream bolts producing a smaller pressure difference across the bolt. However, since there are more bolts, the contribution of pressure-related moment of all bolts together increases.

Figure 21 shows the contribution of skin friction and pressure moment coefficients to the total moment coefficient. It is clear the skin friction contributes less to the overall moment coefficient in comparison with the pressure (which accounts for both form drag and radial pumping).

The dominance of the pressure-related moment means that the net effect of increasing the number of bolts is to (as shown in Figure 21) increase the overall moment coefficient. But for the reasons explained above concerning the structure of the wakes, the rate at which C_m increases with N, decreases as N becomes larger.

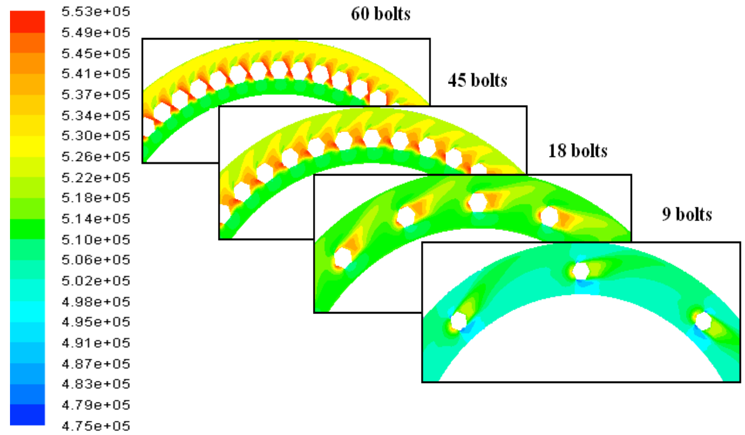

Figure 20. Total pressure Contours around the Bolts for N = 9, 18, 45 and 60 (Re, = 6.8 x 10^6 and C_w = 10^5).

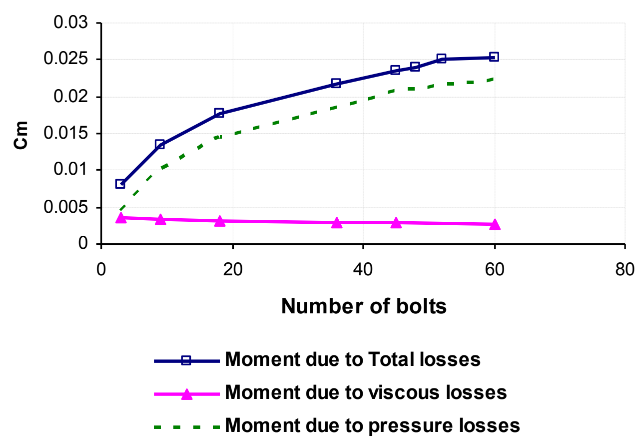

Figure 21. Variation of viscous losses, pressure losses, and total losses with different number of bolts (Re, = 6.8 x 10^6 and C_w = 10^5).

It is also worth investigating the influence of bolts on the flow structure in the rotor-stator cavity. Figure 22 shows the velocity streamlines in the r-z plane on the centreline of the bolthead. Two cases are shown: a plain disc and of a cavity with bolt. And it can be seen that the overall flow has a similar structure for both. There is a recirculation of flow near the stator at the inlet, and another near the exit. However, the exit recirculation is larger in the case of the bolt.

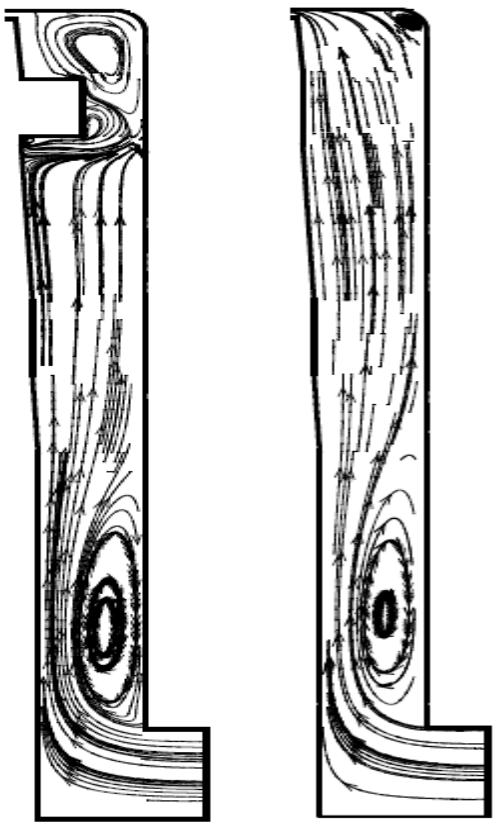

Figure 22. Velocity Streamlines for Re_ϕ = 6.8 x 10^6 and C_w = 10^5.

Left: rotor-stator cavity with bolts
Right: plain rotor-stator cavity

CONCLUSIONS

This paper has presented CFD predictions of the flow in a rotor-stator cavity with and without rotor-mounted bolts. Comparison is made with experimental data for Re_ϕ = 6.8 x 10^6, $C_w = 10^5$ ($\lambda_T = 0.35$), with N = 3, 9 and 18, 16 mm diameter, 11 mm high hexagonal bolts. The number of bolts in the CFD model has been varied from $0 \le N \le 60$ and the contributions of the skin friction and the pressure loss to the overall moment coefficient have been investigated.

The CFD model uses the FLUENT commercial software and a standard K-ε turbulence model. The experimental rig comprises a pressurised rotor-stator cavity of the following geometry: b = 0.225 m, s = 0.022 m, supplied with air.

There is acceptable agreement between the experimental and predicted values of moment coefficient for N = 3, 9 and 18. There is very little difference between the moment coefficient for a continuous ring and that for a plain disc. Increasing the number of bolts brings about an increase in the overall moment coefficient. However, the rate of increase of C_m with N reduces as N gets larger. The tangential velocity between the rotor and stator also increases with N and this causes a reduction in the contribution of skin friction to the overall moment coefficient. The size and shape of the wake formed by a bolts changes with the number of bolts and the wake trailing behind one bolt affects the flow field around a neighbouring bolt. Although the pressure loss per bolt reduces with the number of bolts, the overall effect of increasing N is to increase the overall contribution of pressure loss because there are more bolts.

REFERENCES

Bayley, F.J., Owen, J.M., 1969, “Flow between a rotating and a stationary disc”, Aeronautical Quarterly, Vol. 20, pp.333-354.

Coren, D., 2007. *Windage due to Protrusions in Rotor-Stator Systems*, D.Phil. thesis, Thermo-Fluid Mechanics Research Centre, University of Sussex, Brighton, UK.

Daily, J. W. and Nece, R. E. *Chamber dimension effects on induced flow and frictional resistance of enclosed rotating discs*. J. Basic Eng., 1960, 82, 217–232.

Dibelius, G., Radtke, F., Ziemann, M., 1984. *Experiments on Friction, Velocity and Pressure Distribution of Rotating Discs, Heat and mass transfer in rotating machinery*. (A86-24451 09-34), Washington, DC, Hemisphere Publishing Corp., pp. 117-130.

Gartner, W. 1997 A Prediction Method for the Frictional Torque of a Rotating Disc in a Stationary Housing with a Superimposed Radial Outflow. ASME Gas Turbine and Aeroengine Congress and Exposition, Paper No. 97-GT-204.

Gartner, W., 1998. *A Momentum Integral Method to Predict the Frictional Torque of a Rotating Disc with Protruding Bolts*, ASME conference paper, 98-GT-138.

Millward, J.A., Robinson, P.H., 1989. *Experimental Investigation into the Effects of Rotating and Static Bolts on Both Windage Heating and local Heat Transfer Coefficients in a Rotor-Stator Cavity*, Gas turbine and aeroengine congress and exposition paper, 89-GT-196.

Owen, J. M., Rogers, R. H., 1989, “Flow and Heat Transfer in Rotating-Disc Systems.” Volume one – Rotor-Stator Systems, Research Studies Press Ltd., ISBN 0 86380 090 4.

Pincombe, J.R., 1981. *Velocity Measurements in the MKII – Rotating Cavity Rig with a Radial Outflow*. Report No. 81/TFMRC/21, Thermo-Fluid Mechanics Research Centre, University of Sussex, Brighton, UK.

Poncet, S., Chauve, M.P., Schiestel, R., 2005. “Batchelor versus Stewartson flow structures in a rotor-stator cavity”, Physics Of Fluids, 17, 075110,

von Kármán, T., 1921, “Technical Memorandum on Laminar and Turbulent Friction”, National advisory committee for aeronautics, Report No. 1092.

Zimmerman, H., Firsching, A., Dibelius, G.H., Ziemann, M., 1986. *Friction Losses and Flow Distribution for Rotating Discs with Shielded and Protruding Bolts*, ASME conference paper, 86-GT-158.